Fluid Flow and Thermal Features of Gas Foil Thrust Bearings at Moderate Operating Temperatures

Abdelrasoul M. Gad and Shigehiko Kaneko

Abstract This study aims to analyze the flow characteristics and the thermal features of foil thrust bearing. The flow in the gas film is modeled with 2D compressible Reynolds equation including effects of centrifugal forces in the gas film. The Couette Approximation is adopted for the analysis of temperature distribution in the gas film, and the small perturbations method is used to calculate its dynamic force coefficients. The results show that the Couette Approximation can be used to calculate the temperature distribution in foil thrust bearing with reasonable accuracy and the analysis of the fluid flow reveals that most of the side-leakage occurs in the low-temperature converging region removing less than 5 % of the heat generated in the gas film. Furthermore, with the proper control of cooling flow rate through the bump foils, more than 70 % of the heat generated in the gas film can be removed.

Keywords Foil thrust bearing · Thermal elastohydrodynamic lubrication · Static and dynamic characteristics

1 Introduction

Compliant foil thrust bearings are promising bearings for high speed and high temperature turbomachinery. The compliant bearing is composed of a smooth top foil resting on one or more of flexible corrugated foils called bump foil strips [1],

A.M. Gad (✉)
Faculty of Engineering, Department of Mechanical Engineering,
Assiut University, Assiut, Egypt
e-mail: gad@fiv.t.u-tokyo.ac.jp1

A.M. Gad · S. Kaneko
Department of Mechanical Engineering, School of Engineering,
University of Tokyo, Tokyo, Japan
e-mail: kaneko@mech.t.u-tokyo.ac.jp2

as shown schematically in Fig. 1a. The configuration studied here was described by Dellacorte and Valco [2] as Generation II foil bearings. Compared with foil journal bearings, few studies are found in the open literature concerning the performance of foil thrust bearings. Among these researches, the earliest study of Heshmat et al. [1] about the effects of geometrical parameters and bearing compliance on the bearing load, and the study of Iordanoff [3] about a rapid design method for maximum load carrying capacity. Later, Heshmat et al. [4] investigated the load capacity of foil thrust bearing using an approach which combines Finite Difference and Finite Element methods. With a similar bearing configuration, Park et al. [5] studied the static and dynamic characteristics of foil thrust bearing. Recently, Bruckner [6] analyzed the static characteristics of foil thrust bearing using modified Reynolds equation along with the energy equation. Also, Dykas [7] carried out thorough experiments and reported that both smooth, low friction surfaces combined with adequate thermal management is necessary to support large loads at high rotation speeds. Interesting experimental work on Generation II foil thrust bearing was carried out by Dickman [8] and concluded that the load capacity increases linearly with the speed until thermal effects cause top foil distortions and thermal runaway. Among the recent few studies about the performance of foil thrust bearings, those of Lee and Kim [9, 10] on a hybrid air foil thrust bearing with radially arranged bump foils and the test facility developed by Lee et al. [11] to determine the relation between load capacity and deflection of the compliant bearing. Most recently, Gad and Kaneko [12] have introduced a new structural stiffness model that was applied successfully to predict the static characteristics of Generation II foil thrust bearings. Later, Gad and Kaneko [13] have introduced variable thickness bump foil strips that
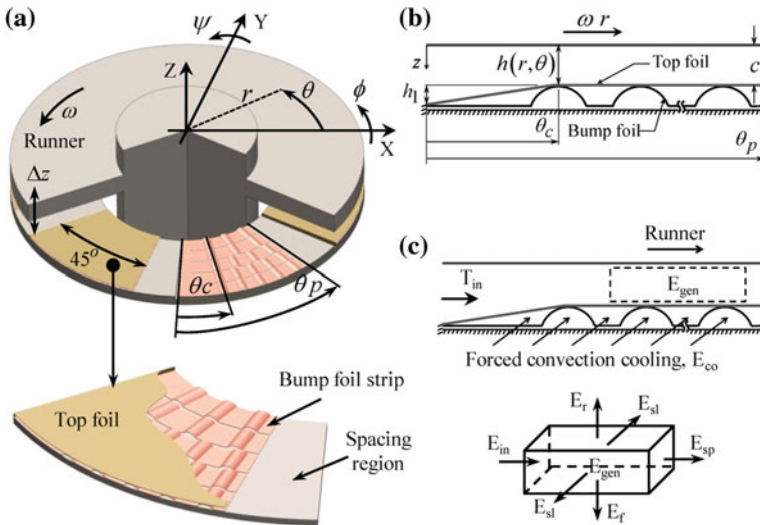
Fig. 1 Generation II foil thrust bearing. **a** Geometry of foil thrust bearing. **b** Geometry of gas film. **c** Thermal energy components

could enhance the load capacity of foil thrust bearing significantly. However, so far, very few studies have handled the flow characteristics along with the thermal features of foil thrust bearings which are essential for the proper design of these bearings. In this study, the flow in the gas film is modeled with 2D compressible Reynolds equation. The Couette Approximation is adopted for the analysis of temperature distribution in the gas film, and the small perturbations method is used to calculate its dynamic force coefficients.

2 Mathematical Model

2.1 Fluid Flow and Bearing Compliance Models

In the present study, the fluid flow in the gas film is modeled using Navier-Stokes and continuity equations in cylindrical coordinates. The introduced flow model follows that of Pinkus and Lund [14] and extends to model the compressible flow in the thin gas film. Hence, the 2D compressible Reynolds equation containing effects of centrifugal forces in the gas film is expressed in non-dimensional form as:

$$
\begin{aligned}
&\frac{\partial}{\partial r}\left(\frac{rph^3}{\mu}\frac{\partial p}{\partial r}\right) + \frac{1}{r}\frac{\partial}{\partial \theta}\left(\frac{ph^3}{\mu}\frac{\partial p}{\partial \theta}\right) = \Lambda\frac{\partial}{\partial \theta}(rph) + 2\Lambda\gamma\frac{\partial}{\partial t}(rph) \\
&+ \frac{\Lambda Re}{20}\frac{\partial}{\partial r}\left(\frac{p\rho r^2 h^3}{\mu}\right) + \frac{9Re}{140\Lambda}\frac{\partial}{\partial r}\left[\frac{p\rho h^7}{r^2\mu^3}\left(\frac{\partial p}{\partial \theta}\right)^2\right] - \frac{Re}{10}\frac{\partial}{\partial r}\left(\frac{p\rho h^5}{\mu^2}\frac{\partial p}{\partial \theta}\right)
\end{aligned}
\tag{1}
$$

where Λ and Re represent the bearing number and modified Reynolds number, respectively, and γ represents the whirl frequency ratio. The dimensionless film thickness (h), see Fig. 1b, can be expressed as;

$$
h(r,\theta) = \begin{cases} 1 + H(1 - \theta/\theta_c) + \delta(r,\theta), \ 0 \leq \theta \leq \theta_c \\ 1 + \delta(r,\theta), \ \theta_c < \theta \leq \theta_p \end{cases}
\tag{2}
$$

where, $\delta(r,\theta) = \delta/c$, $H = h/c$ are the non-dimensional top foil deflection and film thickness ratio, respectively. In the present study, the structural stiffness model introduced by Gad and Kaneko [12] is adopted.

2.2 Thermal Analysis

The steady state temperature distribution in the thin gas film is calculated using the Couette Approximation technique. The technique was developed by Pinkus and Bupara [15] and is based on the assumption that the effect of pressure gradients on the

shear rate of the fluid is much smaller compared with the runner drag effect. The Couette Approximation was applied successfully for predicting the temperature distribution in the air film of compliant foil journal bearing and compliant foil seals [16, 17]. Accordingly, the temperature distribution in the air film is expressed as, [17]:

$$T(r,\theta) = \beta + (T_{in} - \beta)e^{G(r,\theta)} \tag{3}$$

where, $G(r,\theta) = \left(2\alpha\omega/\rho C_p\right)(r/c)^2 \int\limits_0^\theta (c/h)^2 d\theta$

Following the thermal analysis of foil journal bearing introduced by Salehi et al. [17], the energy balance for the control volume shown in Fig. 1c can be written as:

$$E_{in} + E_{gen} = E_{sl} + E_{sp} + E_r + E_f \tag{4}$$

where, E_{in} and E_{gen} refer to the energy of the inlet flow and the energy generated by viscous drag in gas film. Also, E_{sl} and E_{sp} represent the thermal energy carried away by side leakage (at inner and outer boundaries) and at the spacing region between successive bearing pads. Finally, E_r and E_f represents the heat conducted to the runner and the bump foil, respectively. In foil thrust bearing cooling air is passed through the bump foil in the gap between the top foil and the rigid bearing surface so as to remove the heat conducted to the bump foils. This forced convection cooling plays an important role in controlling the bearing temperature as will be explained later in this study.

2.3 Perturbation Method

Similar to Lee and Kim [9] and Park et al. [5], the small perturbations method is applied for the purpose of calculating the dynamic force coefficients of the gas film. The steady state position of the runner is perturbed by small translational displacement (Δz), small rotational displacements ($\Delta\phi$ and $\Delta\psi$), small translational velocity ($\Delta\dot{z}$), and small rotational velocities ($\Delta\dot{\phi}$ and $\Delta\dot{\psi}$) as shown in Fig. 1a. Hence, a set of six perturbation equations is obtained which can be solved for the pressure components once the steady state values of the air film pressure and film thickness are obtained (see Park et al. [5] and Lee and Kim [9] for further details).

2.4 Numerical Methods

The steady state Reynolds equation is discretized using Finite Difference Method and the Newton-Raphson method is used to linearize the discretized equations. The linearized equations are then solved iteratively using Tri-Diagonal Matrix

Algorithm. The fluid model coupled to the structural stiffness model is solved iteratively till the steady state pressure and the corresponding steady state film thickness are obtained. The steady state values are then used to solve the perturbation equations iteratively to calculate the pressure perturbation components which are integrated to obtain the dynamic force coefficients.

3 Results and Discussions

The schematic of the studied foil thrust bearing is shown in Fig. 1a and its geometrical parameters are given in Table 1. For the numerical results presented here, the number of bumps in the bump foil strips was set as 3, 4, 5, 6, and 5 starting from the innermost strip towards the outermost one; an arrangement similar to that used in the experiments of Dickman [8]. The fluid flow and temperature distribution over a single bearing pad is shown in Fig. 2. The velocity field shows clearly that most of the flow that leaks outside the bearing occurs at the converging region of the film. Also, the figure shows that the maximum temperature occurs near the outer edge of the bearing pad as the Couette Approximation assumes the flow temperature to be directly proportional to the radius (r) and inversely proportional to the square of the film thickness (h). Moreover, the results indicate that the peak pressure occurs near the outer region of the pad and the bumps near the free end of the strips experience the largest deflection. The effect of the ramp height (h_1) on the tangential and radial flow velocities is shown in Fig. 3. It is clear from the figure that the increase of the ramp height causes a backflow to occur which in turn decreases the hydrodynamic pressure and the corresponding load carrying capacity of the bearing.

Moreover, the increase of the ramp height increases the side leakage at the convergent region. The most important notice from this figure is that the radial velocity in the converging zone is much higher than that in other regions which indicate that most of the high temperature fluid is entrapped inside the bearing

| Table 1 Geometrical parameters of the studied foil thrust bearing | | |
|---|---|
| Inner radius (mm) | 25 |
| Outer radius (mm) | 50 |
| Number of bearing pads | 6 |
| Bump foil angular extent (°) | 45 |
| Top foil angular extent (°) | 45 |
| Number of bump foil strips/pad | 5 |
| Top foil thickness, t_f (mm) | 0.1524 |
| Bump foil thickness, t_b (mm) | 0.102 |
| Bump radius, R (mm) | 1.5875 |
| Bump height, h_b (mm) | 0.508 |
| Young's modulus of bump foil, E (GPa) | 214 |
| Poisson's ratio of bump foil, v | 0.29 |
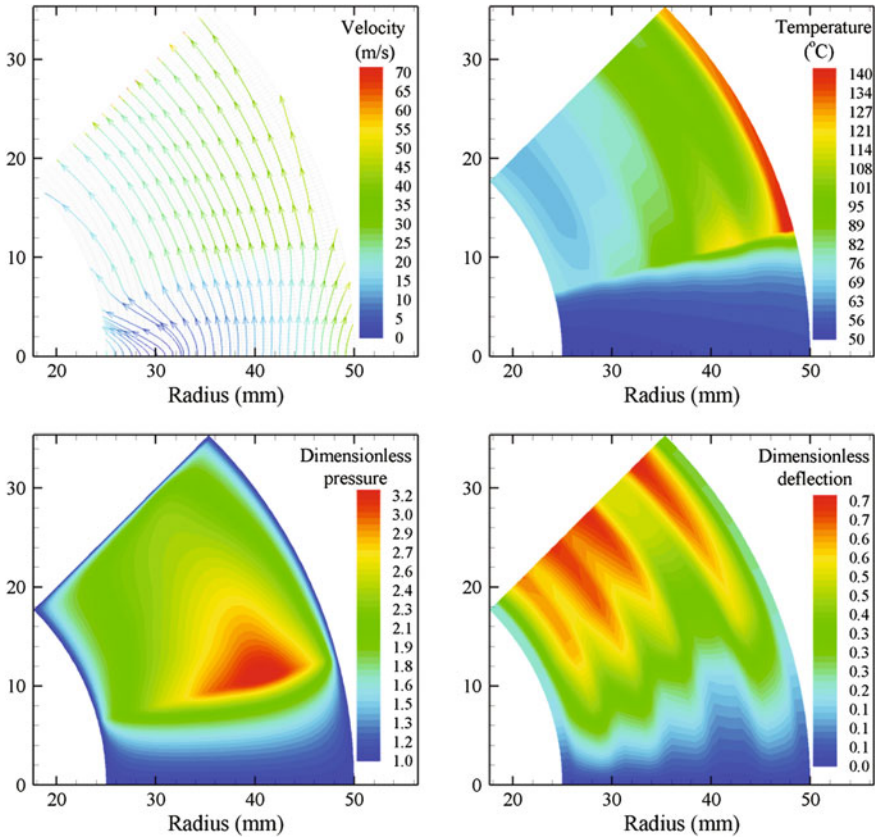
Fig. 2 Fluid flow and temperature distribution in foil thrust bearing ($c = 5\,\mu m$, $\omega = 40$ krpm, $T_{in} = 50\,°C$)

cavity. These results agree well with a previous analysis by Gad and Kaneko [12] who reported that the foil thrust bearing with a film thickness ration (H) of 4 can achieve the highest load carrying capacity. The variation of the viscous friction torque with bearing load at different inlet temperatures is shown in Fig. 4a. The results from this figure can be explained by realizing that the viscous friction torque is inversely proportional to the film thickness, and hence increasing the bearing load will cause a corresponding increase in the friction torque as a result of reducing the gas film thickness. Figure 4b shows a comparison between the load carrying capacity obtained with the present analysis and that obtained experimentally by Dickman [8]. The current program code was run at the same operating conditions reported in the experimental study. The comparison shows a good agreement between the present numerical results and those obtained experimentally. However, at higher rotation speed, the numerical analysis overestimates the bearing load capacity. This may be attributed to the thermal runaway and loss of full gas film
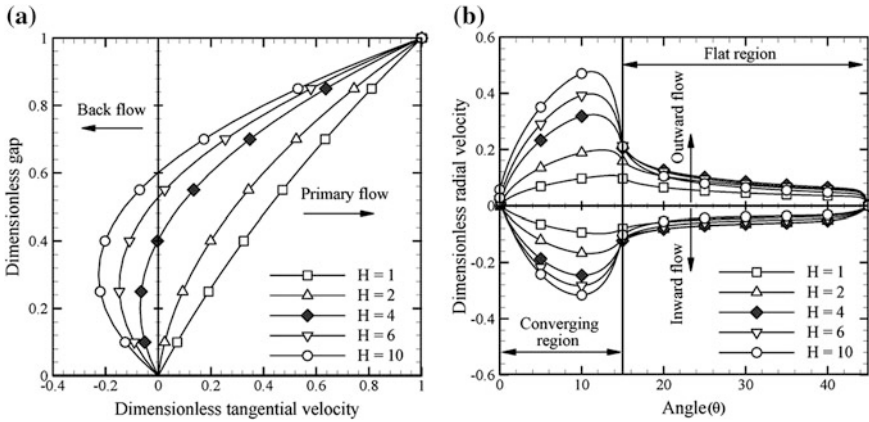
Fig. 3 Fluid flow variation with ramp height, $(c = 8 \, \mu m, \, \omega = 30 \, krpm, \, T_{in} = 25 \, °C)$. **a** Tangential velocity at pad inlet. **b** Radial velocity at inner and outer radii
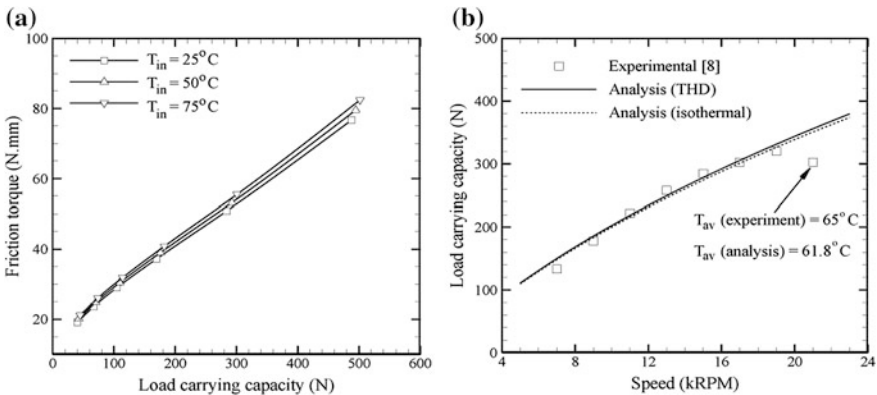

Fig. 4 Foil thrust bearing friction torque and load capacity. **a** Variation of friction torque with bearing load. **b** Comparison with experiments, [8]

which causes the load carrying capacity to decrease. It should be pointed out that the average temperature predicted with the present analysis at such rotation speed is very close to the one measured experimentally. The temperature distribution in circumferential direction at three different radii and with two nominal film thicknesses is shown in Fig. 5a. The results show that the flow temperature increases sharply near the end of the convergent region as a result of the high shear rate there. Also, it can be noticed that the maximum flow temperature at thick gas film occurs near the outer edge of the bearing pad while at very thin gas films the maximum temperature is located near the position of peak pressure. These outcomes are
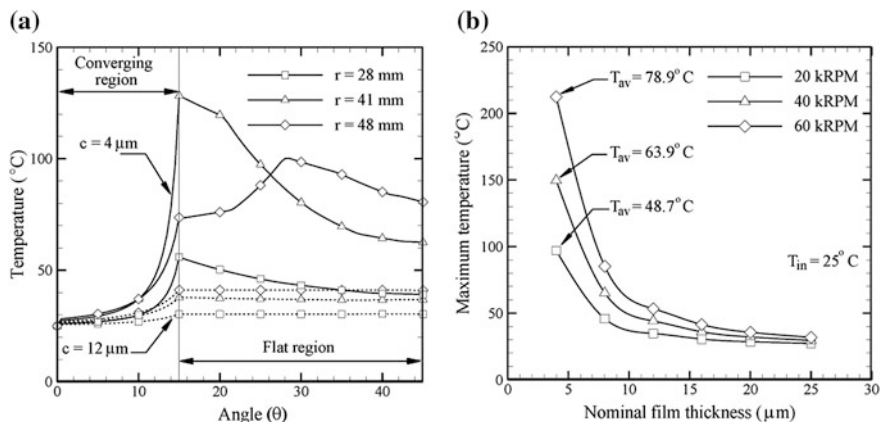
Fig. 5 Thermal features of foil thrust bearing. **a** Temperature distribution in tangential direction. **b** Maximum temperature variation with nominal film thickness
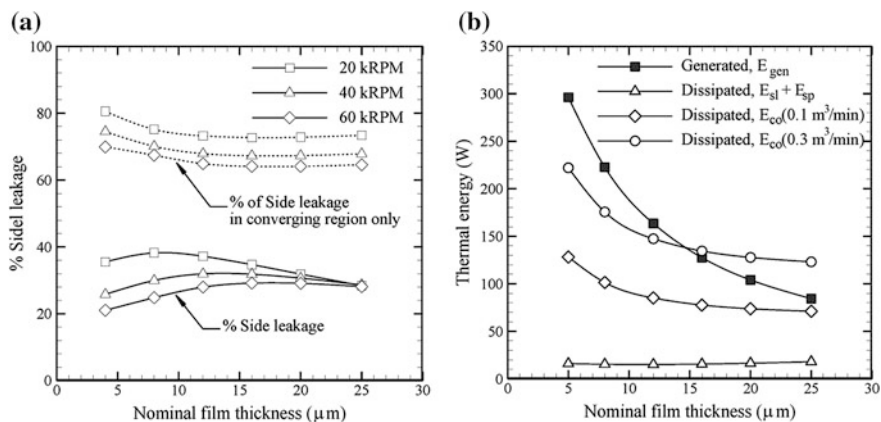

Fig. 6 Side leakage and thermal energy components in foil thrust bearing. **a** Variation of side leakage with nominal film thickness. **b** Thermal energy components and forced convection cooling

emphasized in Fig. 5b which shows that the maximum temperature of the flow increases sharply as the nominal film thickness decreases. Additionally, Fig. 5b shows that increasing the rotation speed increases the shear rate of the fluid which in turn causes the flow temperature to increase. The variation of percent side leakage with nominal film thickness is shown in Fig. 6a for three different rotation speeds. In order to visualize the results of this figure, it is important to declare that the flow in the convergent region of the pad is dragged by the rotating runner and squeezed out as it passes through such narrowing gap. If the drag force is small, much fluid may squeezed out of the film and vice versa. Hence, at high rotation speeds, the percent side leakage decreases as a result of the high drag force even

with very thin gas films. However, at a constant rotation speed, the results shows that the side leakage increases very slowly as the film thickness decreases till a certain value, after which further decrease of the film thickness causes the side leakage to decrease. This is attributed to the fact that the side leakage is inversely proportional to the fluid viscosity, and hence as the film thickness decreases, the fluid temperature increases and, consequently, the fluid viscosity increases which causes the side leakage to decrease.

Another important notice from Fig. 6a is that more than 65 % of the side leakage occurs in the convergent zone only; a feature indicating that the side leakage heat transfer in foil thrust bearing is negligible since most of the fluid that leaks outside the bearing leaves at comparatively low temperature. The ability of forced convection cooling through the bump foil to remove the generated heat from the bearing is shown in Fig. 6b. The figure shows that the side-leakage heat transfer can
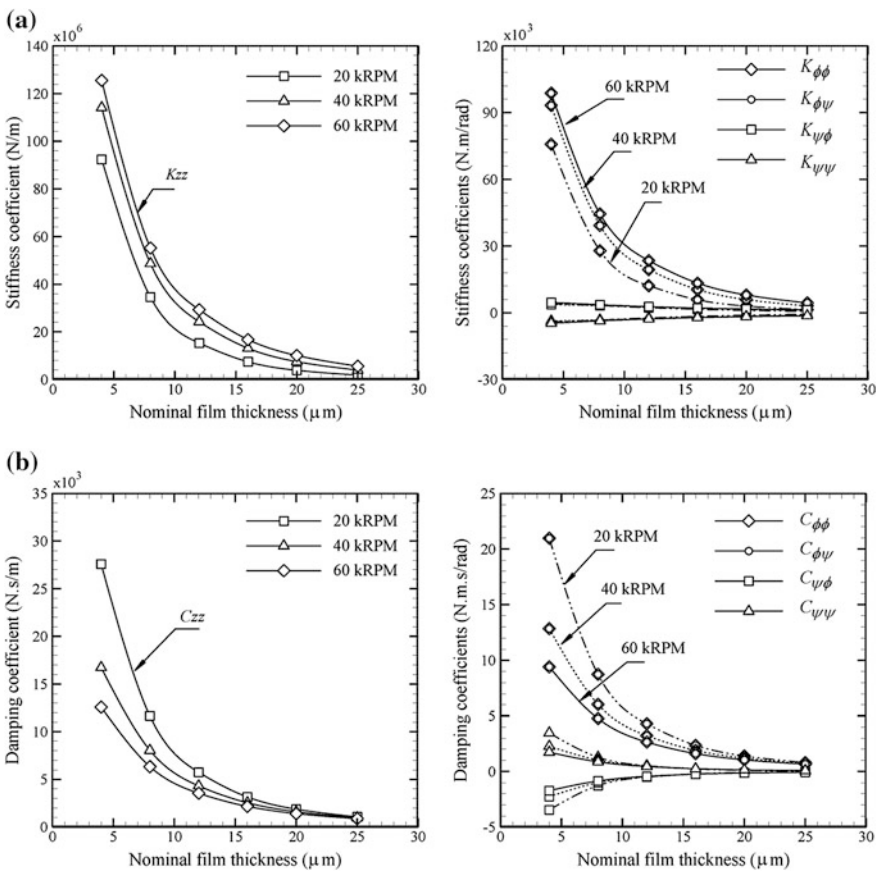
Fig. 7 Variation of stiffness and damping coefficients with nominal film thickness, ($h_1 = 25$ μm, $T_{in} = 25$ °C). a Stiffness coefficients. b Damping coefficients

remove less than 5 % of the heat generated in the bearing. Furthermore, the figure shows that with the proper choice of forced convection cooling flow rate, more than 70 % of the heat generated in the bearing can be removed. The results shows clearly that cooling foil thrust bearings by forced convection through the bump foils can remove most of the heat generated in the bearing. Finally, the variations of stiffness and damping coefficients with nominal film thickness are shown in Fig. 7. Only the variation of stiffness and damping coefficients of considerable magnitude are shown, since the magnitude of other coefficients were found to be negligible [9]. The results from this figure show clearly that the stiffness and damping capabilities of the gas film increases sharply as the nominal film thickness decreases and that the gas film becomes relatively soft at large values of nominal film thickness even with high rotation speeds. Fortunately, as gas-lubricated foil bearings usually operates with minimum film thicknesses of less than 10 μ [2], reasonable stiffness and damping capabilities of these bearings are maintained.

4 Conclusions

In the present study, the fluid flow in Generation II foil thrust bearing is modeled with 2D compressible Reynolds equation including effects of centrifugal forces in the gas film and the Couette Approximation was used to obtain the temperature distribution in the gas film. The small perturbations method was used to evaluate the dynamic force coefficients. The analysis revealed the following remarks:

- The Couette Approximation technique can be used to calculate the temperature distribution in the gas film of foil thrust bearing with reasonable accuracy.
- Most of the flow that leaks out of the bearing occurs in the converging region of the film which exhibit low temperature field and, consequently, it removes less than 5 % of the heat generated in the gas film.
- The forced convection cooling through the bump foils is essential in removing most of the heat generated in the gas film, and with a proper control of the cooling flow rate, more than 70 % of the heat generated in the bearing can be removed.

References

1. Heshmat H, Walowit JA, Pinkus O (1983) Analysis of gas-lubricated compliant thrust bearings. J Lubr Technol 105:638–646
2. Dellacorte C, Valco MJ (2000) Load capacity estimation of foil air journal bearings for oil-free turbomachinery applications. Tribol Trans 43(4):795–801

3. Iordanoff I (1999) Analysis of an aerodynamic compliant foil thrust bearing: method for a rapid design. J Tribol 121(4):816–822
4. Heshmat CA, Xu DS, Heshmat H (2000) Analysis of gas lubricated foil thrust bearings using coupled finite element and finite difference methods. J Tribol 122(1):199–204
5. Park D-J, Kim C-H, Jang G-H et al (2008) Theoretical considerations of static and dynamic characteristics of air foil thrust bearing with tilt and slip flow. Tribol Int 41:282–295
6. Bruckner RJ (2004) Simulation and modeling of the hydrodynamic, thermal, and structural behavior of foil thrust bearings. Ph.D. thesis, Case Western Reserve University, USA
7. Dykas BD (2006) Factors influencing the performance of foil gas thrust bearings for oil-free turbomachinery applications. Ph.D. thesis, Case Western Reserve University, USA
8. Dickman JR (2010) An investigation of gas foil thrust bearing performance and its influencing factors. M.Sc. thesis, Case Western Reserve University, USA
9. Lee D-H, Kim D-J (2011) Design and performance prediction of hybrid air foil thrust bearings. J Eng Gas Turbines Power 133:042501
10. Lee D-H, Kim D-J (2011) Three-dimensional thermohydrodynamic analyses of rayleigh step air foil thrust bearing with radially arranged bump foils. Tribol Trans 54:432–448
11. Lee Y-B, Kim T-Y, Kim C-H et al (2011) Thrust bump air foil bearings with variable axial load: theoretical predictions and experiments. Tribol Trans 54:902–910
12. Gad AM, Kaneko S, A new structural stiffness model for bump-type foil bearings: application to generation ii gas lubricated foil thrust bearing. J Tribol doi:10.1115/1.4027601
13. Gad AM, Kaneko S (2014) CFD-based design and performance characteristics of generation ii foil thrust bearing for microturbomachinery applications. In: Proceedings of ISROMAC-15, Honolulu, HI, USA, 24–28 Feb
14. Pinkus O, Lund JW (1981) Centrifugal effects in thrust bearings and seals under laminar conditions. J Lubr Technol 103:126–136
15. Pinkus O, Bupara SS (1979) Adiabatic solution for finite journal bearings. J Lubr Technol 101:492–496
16. Salehi M, Heshmat H (2000) On the fluid flow and thermal analysis of a compliant surface foil bearing and seal. Tribol Trans 43:318–324
17. Salehi M, Swanson E, Heshmat H (2001) Thermal features of compliant foil bearings—theory and experiments. J Tribol 123:566–571